Loewe, R. (1978) *J. Comp. Physiol. 128*, 161-168.
Loewe, R., Schmid, R., & Linzen, B. (1977) in *Proceedings in Life Sciences: Structure and Function of Haemocyanin* (Bannister, J. V., Ed.) pp 50-54, Springer-Verlag, Berlin and Heidelberg.
Markl, J. (1986) *Biol. Bull. (Woods Hole, Mass.) 171*, 90-115.
Markl, J., Savel, A., Decker, H., & Linzen, B. (1980) *Hoppe-Seyler's Z. Physiol. Chem. 361*, 649-660.
Markl, J., Kempter, B., Linzen, B., Bijlholt, M. M. C., & Van Bruggen, E. F. J. (1981a) *Hoppe-Seyler's Z. Physiol. Chem. 362*, 1631-1641.
Markl, J., Savel, A., & Linzen, B. (1981b) *Hoppe-Seyler's Z. Physiol. Chem. 362*, 1255-1262.
Markl, J., Decker, H., Linzen, B., Schutter, W. G., & Van Bruggen, E. F. J. (1982) *Hoppe-Seyler's Z. Physiol. Chem. 363*, 73-87.
Monod, J., Wyman, J., & Changeux, J. P. (1965) *J. Mol. Biol. 12*, 88-112.
Richey, B., Decker, H., & Gill, S. J. (1985) *Biochemistry 24*, 109-117.
Robert, C. H., Decker, H., Richey, B., Gill, S. J., & Wyman, J. (1987) *Proc. Natl. Acad. Sci. U.S.A. 84*, 1891-1895.
Savel, A., Markl, J., & Linzen, B. (1986) in *Invertebrate Oxygen Carriers* (Linzen, B., Ed.) pp 399-402, Springer-Verlag, Berlin and Heidelberg.
Schartau, W., & Leidescher, T. (1983) *J.* Comp. *Physiol. 152*, 73-77.
Van Bruggen, E. F. J., Schutter, W. G., Jan, F. L., Van Breemen, J., Bijlholt, M. M. C., & Wichertjes, T. (1982) in *Electron Microscopy of Proteins* (Harris, J. R., Ed.) Vol. 1, pp 1-38, Academic, London.
Van Holde, K. E., & Van Bruggen, E. F. J. (1971) in *Subunits in Biological Systems* (Timmasheff, S. N., & Fasman, G. D., Eds.) pp 1-53, Marcel Dekker, New York.
Van Holde, K. E., & Miller, K. (1982) *Q. Rev. Biophys. 15*, 1-129.
Wyman, J. (1964) *Adv.* Protein *Chem. 19*, 223-286.
Wyman, J. (1972) *Curr. Top. Cell. Regul. 6*, 207-223.
Wyman, J. (1984) *Q. Rev. Biophys. 17*, 453-488.
Zolla, L., Brunori, M., Richey, B., & Gill, S. J. (1985) *Biophys. Chem. 22*, 271-280.

Dynamics Simulation Studies of Apoazurin of *Alcaligenes denitrificans*†

Lin X.-Q. Chen,‡,§ Richard A. Engh,‡,∥ Axel T. Brünger,⊥ Dzung T. Nguyen,⊥ Martin Karplus,*,⊥ and Graham R. Fleming*,‡,#

Department of Chemistry, Harvard University, Cambridge, Massachusetts 02138, and Department of Chemistry and James Franck Institute, The University of Chicago, Chicago, Illinois 60637

Received December 21, 1987; Revised Manuscript Received April 28, 1988

ABSTRACT: Molecular dynamics simulations using the stochastic boundary method were carried out for apoazurin of *Alcaligenes denitrificans*. For a region centered on the exposed tryptophyl residue (W118), simulations in vacuo and with inclusion of model water molecules were carried out. The simulations are in accord with the experimental finding that the interior tryptophan (W48) is less mobile than the exterior tryptophan (W118). In simulations with and without solvent the motion of W118 is strongly correlated with residues connected along the backbone and residues close to the face of the indole ring. The 50-ps simulated tryptophan fluorescence anisotropies did not reveal the slowly decaying component (160 ps) found experimentally. Estimates of energy transfer between W48 and W118 give rates similar to the experimental value provided that the initial state is ^1L_b. Variations of rate of ±20% are found when the relative motions of the two residues are taken into account.

The internal motions of protein molecules have generated much interest in recent years because of their possible significance in protein function (Gurd & Rothgeb, 1979; Williams, 1979; Karplus & McCammon, 1981, 1983). A variety of techniques for the study of protein dynamics have been developed including high-resolution X-ray diffraction (Petsko & Ringe, 1984; Debrunner & Frauenfelder, 1982; Artymiuk et al., 1979), NMR (Richarz et al., 1980; Gall et al., 1981, 1982; Rice et al., 1981; Dobson & Karplus, 1986), time-resolved optical spectroscopy (Hochstrasser & Negus, 1984; Lakowicz et al., 1983; Munro et al., 1979; Petrich et al., 1987), and molecular dynamics (MD) computer simulation (Karplus & McCammon, 1981, 1983; van Gunsteren & Karplus, 1982; Ichiye & Karplus, 1983). Improvements in time-resolved spectroscopy and computers are extending the time scale of both experiment and theory, so that direct comparisons should be possible in the near future; i.e., subnanosecond events may be measured by spectroscopic methods, and molecular dynamics simulations have been extended into the nanosecond time scale. The information concerning the atomic motions provided by MD simulations can assist in the interpretation of experimental results, and the reliability of both the experimental and theoretical techniques can be tested by appropriate comparisons. It has been shown, for example, that the standard interpretation of the temperature factors in the X-ray analysis of proteins can result in significant errors in the estimates of side-chain motions (Yu et al., 1985; Kuriyan et al., 1986). The validity of the interpretation of NMR

† This work was supported by a grant from the National Science Foundation (to G.R.F. and M.K.). We also thank the National Science Foundation for the computation time on CRAY-1 and CRAY-2 supercomputers and the service provided by University of Minnesota Supercomputer Center. The Evans & Sutherland graphic system PS300 was provided by NSF Grant PCM-8304504.
‡ The University of Chicago.
§ Present address: Department of Chemistry, University of California at Berkeley, Berkeley, CA 94720.
∥ Present address: Max-Planck-Institut für Biochemie, D-8033 Martinsreid bei München, West Germany.
⊥ Harvard University.
John Simon Guggenheim Fellow.

0006-2960/88/0427-6908$01.50/0

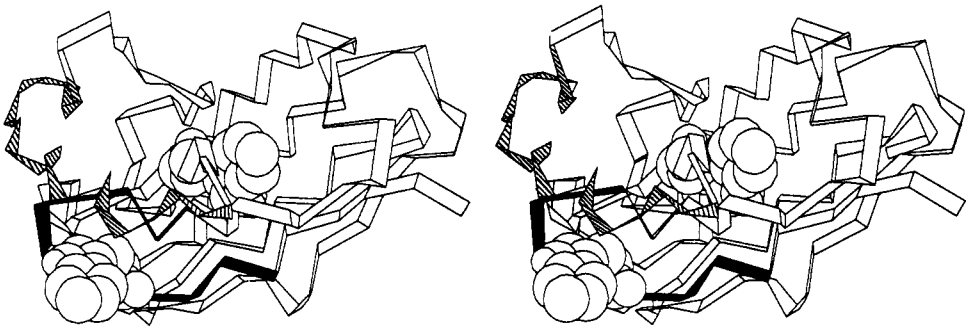

FIGURE 1: Stereo diagram of apoazurin *A. denitrificans*. The backbone is displayed as a ribbon to show the secondary structure elements more clearly, and the two tryptophan residues are depicted as CPK model structures. Tryptophan 48 is part of a β-barrel structure, and its side chain is located in the interior of the barrel surrounded by other hydrophobic residues. Tryptophan 118 is part of a very short helical segment (shaded in solid dark) on the surface of the protein and is adjacent to the α-helical segment (shaded with lines) of the molecule.

parameters (T_1, T_2, and NOE data) has also been examined by the use of simulation methods (Dobson & Karplus, 1986). Henry et al. (1985) simulated ligand photodissociation from hemoglobin and the cooling in laser-excited heme proteins (Henry et al., 1986). The simulations are in accord with the analysis of subpicosecond spectral changes on ligand dissociation as well as the interpretation of the Raman spectra of heme proteins.

Time-resolved optical spectroscopic techniques for probing local motions of macromolecules generally rely either on bound chromophores or those that are intrinsic to the system of interest. Excitation with polarized light creates an anisotropic distribution of chromophores, and the time evolution of this photoinduced anisotropy can be correlated with local and global motions (Demchenko, 1986). Tryptophan residues, present in many proteins and naturally occurring peptides, provide intrinsic nonperturbing probes for internal motions of proteins. However, the photophysics of tryptophan residues (Creed, 1984; Longworth, 1972) complicates the analysis of experimental measurements. For example, the two lowest lying singlet excited states have overlapping transition energies and shift relative to each other depending on environment. The orientations of the transition dipoles also have not been determined exactly, although a variety of experiments have provided estimates of the orientations in the gas phase (Philips & Levy, 1986) and in crystalline environments (Negus, 1985). Nevertheless, the fact that its fluorescence properties are influenced by the environment of the residue and that the decay of the photoinduced anisotropies can be measured relatively easily makes tryptophan useful as a probe for protein structure and mobility (Demchenko, 1986). In solution, multiple exponential lifetimes indicate complex excitation decay kinetics that most likely involve several distinct excited species. Solution studies have led to models that associate different fluorescence properties with different dihedral conformers (Chang et al., 1983; Petrich et al., 1983; Fleming et al., 1978; Engh et al., 1986); conformers may have similar effects in a protein environment. A molecular dynamics simulation of tryptophan mobilities in egg white lysozyme (Ichiye & Karplus, 1982) has been used to calculate correlation functions of transition dipole orientations and to analyze possible contributions to experimentally determined anisotropy decays.

In this paper, we consider the tryptophan motion in the apoazurin protein of the bacterium *Alcaligenes denitrificans* (Ade). Azurin ade is a blue-copper electron-transfer protein containing 129 amino acids. Its structure has been determined by X-ray crystallography and refined to a resolution of 2.0 Å (Norris et al., 1983). The coordinates are available from the Brookhaven Protein Data Bank (Bernstein et al., 1977). Azurin Ade is an ellipsoidal molecule (see Figure 1) with one tryptophan residue (Trp 118) on the surface and another tryptophan residue (Trp 48) in the core of the protein; i.e., the indole moiety of Trp 118 is partially exposed to the solvent, while that of Trp 48 is deeply buried in the β-barrel core with two β-sheets packed face to face (Norris et al., 1986) and has a fluorescence emission maximum at 308 nm at room temperature (Finazzi-Agro et al., 1970, 1973). This is the most blue-shifted spectrum known among tryptophan residues in proteins (Longworth, 1971), and is in accord with the highly hydrophobic environment surrounding the residue.

The fluorescence lifetimes and anisotropies of several azurin proteins have been studied by Petrich et al. (1987). The anisotropy decay measurements indicate that the two tryptophan residues differ in mobility. The azurin of *Alcaligenes faecalis*, which has only the exterior Trp 118, showed a biexponential rotational correlation decay with a short time component of 160 ps, indicating restricted motion on this time scale. The azurin of *Pseudomonas aeruginosa* has only the interior Trp 48 and showed only a single-exponential anisotropy decay, with a decay time of 5 ns corresponding to the overall rotation; there was no measurable internal motion (simulated data showed that free diffusion in a cone with semiangle $<22°$ is not detectable in these experiments; see Petrich et al., 1987). The fluorescence of apoazurin Ade at the red edge of the emission spectrum showed a rise time of 0.9 ns in addition to a 3.8-ns decay time. This rise time is very likely a result of energy transfer from Trp 48 to Trp 118.

To compare these experimental measurements with molecular simulations and to estimate the effects of dynamics on energy transfer, we have performed molecular dynamics simulations for azurin Ade. Because Trp 118 is accessible to the solvent in the X-ray structure, the simulations are best performed with explicit inclusion of solvent molecules. However, a full simulation of the solvated protein requires excessive computer time. To reduce the problem, the stochastic boundary molecular dynamics method (SBMD) (Brooks et al., 1983, 1985) was used. Previous work (Brooks et al., 1985) has shown that if the boundary is properly selected, the local structure in the center of the SBMD region is very similar to that in the full simulation. This makes it possible to simulate a localized portion of the protein surrounded by solvent molecules. For the simulations, we selected two regions of the protein, each centered on one of the tryptophan residues. For the region centered on the exterior Trp 118, two types of simulations were done; one of these was a vacuum simulation, and in the other the tryptophan was surrounded by solvent. For the interior Trp 48, the stochastic boundary is defined so that the simulation region is entirely within the protein.

Descriptions of the method and of the three simulation systems, including the SBMD parameters selected for these

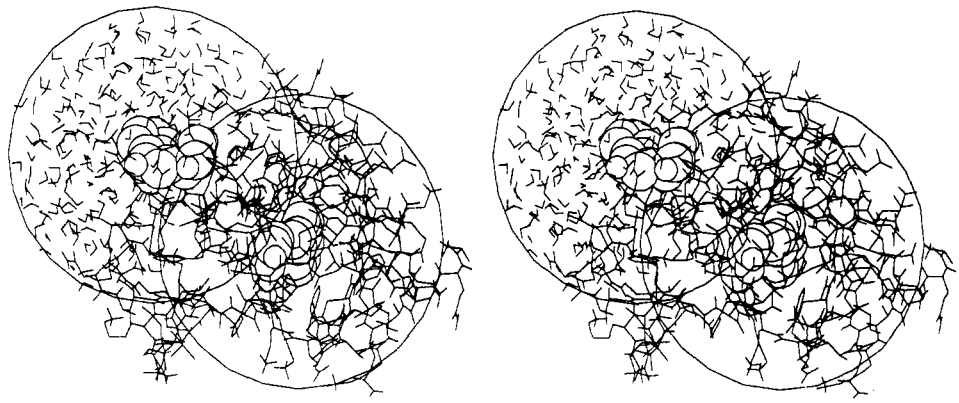

FIGURE 2: Stereo diagram of the energy-minimized structure and simulation regions of azurin Ade. The TIP3P solvent molecules of W118V are also displayed. The solid circles indicate the approximate areas simulated; the dotted circles indicate the reaction region–buffer region boundaries. Tryptophan residues are displayed with a CPK type image for clarity. The figure was created by using programs of Lesk and Hardman (1982) adapted for use with the NCAR graphics system.

simulations, are given under Methods. Under Results and Discussion, we first present a brief description of the general features of the atomic fluctuations. An analysis of the tryptophan motions is then given, and the effect of the solvent on the simulation results is described. Finally, we present an analysis of the dependence of energy transfer between the tryptophan residues on their internal motions.

METHODS

The macromolecular simulation program CHARMM (chemistry at Harvard molecular mechanics) (Brooks et al., 1983) was used for the simulations. The stochastic boundary molecular dynamics (SBMD) method (Brooks et al., 1983, 1985) was used to generate dynamics trajectories for three systems: the core region of azurin Ade centered on Trp 48, a surface region of azurin Ade centered on Trp 118 with solvent, and the same surface region without solvent. In this section, we describe the details of the simulation method that are unique to these systems. SBMD divides a large system into three regions: the reaction region, the buffer region, and a reservoir region. The region of interest is contained within the reaction region, where all atoms are treated with classical molecular dynamics (Brooks et al., 1985). The atoms in the outermost region, the reservoir region, are not included in the simulation. In the buffer region, atoms are included explicitly and are treated with classical Langevin dynamics; i.e., terms that approximate the systematic and stochastic forces that would arise from interactions with atoms in the reservoir region are added to the standard molecular dynamics equation. Restoring forces on the protein buffer region atoms are determined from high-resolution diffraction studies. They minimize distortions arising from truncation of the external atoms. For the solvent, an average boundary force is introduced (Brünger et al., 1984). A more complete description of the method can be found elsewhere (Brooks et al., 1985).

The 2.0-Å resolution X-ray structure for azurin Ade by Norris et al. (1983), available from the Brookhaven Protein Data Bank, provided the initial coordinates for the simulation. Azurin Ade (see Figure 1) approximates an ellipsoid with dimensions 25 Å × 30 Å × 40 Å. The two tryptophan residues are separated by approximately 13 Å. The Cu(II) prosthetic group is approximately 11 Å from each residue. To simulate the apoazurin, the copper atom was deleted from the coordinates on the assumption that the effect of copper on tryptophan motion is negligible. The strain introduced by the deletion was relaxed by energy minimization.

The CHARMM 19 force field was used for the simulations. All atoms except aliphatic hydrogens were included; the aliphatic C–H groups were treated as single "extended atoms" (Brooks et al., 1983a). Polar hydrogens and other atoms that were not defined by the X-ray structure were generated and patched into the structure. Prior to the dynamics simulation, 40 cycles of energy minimization using the conjugate gradients method (Fletcher et al., 1964) were applied to the whole protein to relax local strains in the X-ray structure and those arising from the deletion of the copper atom.

Two simulation systems were generated, each centered on a tryptophan residue at the mean position of the tryptophan side chain atoms. Figure 2 shows the relationship of the simulation regions to the entire protein. The radius of the reaction region (12 Å) for each system was selected such that the tryptophan residue would remain in the reaction region for all reasonable motions. The radial thickness of the buffer regions was 2 Å; all atoms at a distance greater than 14 Å from the relevant tryptophan residue were eliminated. Any atoms on a boundary were considered to belong to the inner region. Atoms of the same side chain were not partitioned into different regions, but were assigned to the innermost part of the appropriate regions. Backbone atoms were assigned individually to the appropriate regions. A table showing the initial assignments of the atoms to the particular regions is available from the authors on request. A list of initial assignments of the individual residues is given in footnote *b* of Table I.

The interior Trp 48 simulation contained 830 atoms, of which 566 were in the reaction region and 264 were in the buffer region initially. All of the buffer region is inside the protein. The molecular structure in this system is largely composed of β-strands, which are the part of the β-barrel in the middle of the molecule. Trp 48 is surrounded mostly by apolar residues, including Leu 34, Val 23, Val 59, and Phe 61. This mostly hydrophobic environment blue shifts the tryptophan emission spectrum. The molecule is closely packed in this region, so it is unlikely to allow penetration of solvent molecules. Thus, no water molecules were included. This system was given the mnemonic W48.

The Trp 118 system without solvent contained 458 atoms, of which 306 were in the reaction region and 152 were in the buffer region initially. The molecular structure in this system is composed of an α-helix and a few turn or loop structures. Trp 118 is largely exposed to solvent and is close to a few polar residues including Glu 57, Lys 56, and Met 64. This system was given the mnemonic W118V.

The Trp 118 system with solvent water molecules was generated by overlapping the Trp 118 centered system with a rectangular box of equilibrated TIP3P (Jorgensen, 1981)

water molecules. Solvent molecules that were located either within 2.60 Å of any protein atom or outside the 14-Å sphere radius (centered at Trp 118) were deleted. This system was given the mnemonic W118S.

The systems without solvent were each equilibrated for 8 ps. The equilibrations were carried out in the same manner as the simulations themselves. The Verlet algorithm (Verlet, 1967) with a step size of 1 fs was used to integrate the equations of motion derived from these potentials. As already mentioned, atoms in the buffer region were treated with the Langevin equation; i.e., additional stochastic forces and harmonic restraining potentials were used (Brooks et al., 1985). These additional terms were scaled according to the proximity of the atoms to the reservoir region. The boundary region was divided into four subshells of 0.5-Å thickness, and a scaling factor for each subshell was assigned to atoms in the appropriate subshell. This scaling factor reflects the relative importance of the forces that would arise from the eliminated reservoir atoms and those from the explicitly included buffer and reaction region atoms. The stochastic forces are scaled from 0.5 at the buffer/reservoir boundary to zero at the reaction/buffer boundary. This treatment of stochastic forces was shown to produce good results for active-site simulations of BPTI (Brünger et al., 1984). The harmonic restoring forces were chosen on the basis of X-ray temperature factor values for azurin Ade (Norris et al., 1984). The B factors from the X-ray analysis were averaged over each atom type (e.g., C_α, C_β, ..., N_ϵ, O, etc.). The harmonic force constant for each atom in the buffer region was chosen via the equation

$$k_{\mathrm{har}}{}^{i} = \frac{4\pi^2 k_B T}{B_i} S_i \qquad (1)$$

where S_i is the scaling factor for the ith atom and B_i is the average B factor for this type of atom. The stochastic dynamics friction coefficient (Brooks et al., 1985) was chosen to be 200 ps^{-1}, scaled according to the buffer subshell. This choice was based on previous protein simulations and the calculated velocity autocorrelation functions (Brooks et al., 1985).

For the system W118S, in addition to the protein atoms in the boundary region, which were treated in W118V, there were water molecules in the boundary region. A friction coefficient of 62 ps^{-1} with appropriate scaling was assigned to these water molecules (Brooks et al., 1983b). Also, a restraining potential (Brünger et al., 1984) was added at the reservoir boundary to confine the water molecules to the simulation regions. The equilibration of W118S was performed in two steps. After introduction of water molecules, an 8-ps equilibration of the water molecules was performed with the protein coordinates kept fixed. This was followed by an additional 8-ps equilibration in which all atoms (protein and solvent) were allowed to move. After the second equilibration was completed, it was found that the system had shrunk somewhat, and there was room to add 13 more solvent molecules. In all, 223 water molecules were included in W118S for a total of 1127 protein plus water atoms.

The temperature of the simulations was set equal to 300 K; this temperature was used in the Langevin equations. The coordinates were recorded every 50 time steps. The Langevin atom list and the associated values of the position-dependent Langevin parameters were updated every five steps for all atoms. The nonbonded interactions were calculated within an 8.0-Å radius. A switching function continuously switched off the interactions from 7.5 to 8.0 Å. A nonbonded list of pairs within 9.0 Å was generated and updated every 20 steps. The larger radius used in the determination of the pair list prevents the introduction of impulsive forces when the pair list is updated.

Table I: rms Difference between Simulations and X-ray Structure[a,b]

simulation	backbone atoms	side-chain atoms
W118S	0.783 (0.478)	1.675 (0.558)
W118V	1.020 (0.501)	2.715 (1.136)
W48	0.739 (0.808)	1.774 (0.767)

[a] All values in angstroms. The numbers correspond to the atoms in the reaction region (unconstrained molecular dynamics) and those in parentheses to the atoms in the buffer region (constrained Langevin dynamics). [b] The following residues were included, at least in part, in the reaction region: for W48, 3–9, 15–22, 29–34, 46–53, 56, 59, 71, 73, 79–87, 92–98, 102, 108–114, and 121–126; for W118, 13, 15, 47, 49, 51–65, 72, 79, and 109–123. In the buffer region residues included the following: for W48, 1, 3, 9–10, 14–16, 22–23, 28, 35–46, 45–46, 52–53, 55–56, 59–60, 71–73, 77, 79, 86–87, 91–92, 98–99, 101–102, 106–107, 113–114, 117–118, 120–121, and 127; for W118, 13–15, 45–54, 64–67, 71–74, 77, 79–80, 109, and 123. Some residues appear partly in the reaction and in the buffer regions.

After equilibration, a 50-ps SBMD trajectory was generated for each of the three systems. An additional 10-ps simulation was generated for each system to examine the convergence of total energy, χ_1 and χ_2 dihedral trajectories, and fluctuations. The equilibrations and dynamics trajectories were all performed on the Cray-1 on the Minnesota Supercomputer Center. To generate 10 ps of dynamics, approximately 50 min was required for W118V (458 atoms), 220 min for W118S (1127 atoms), and 100 min for W48 (830 atoms). Most of the analysis was done on the Cray-2 at the Minnesota Supercomputer Center.

In order to compare the protein structures during the dynamics runs with the X-ray structure, we calculated rms differences between the simulation and X-ray structures for atoms in the active and buffer regions. The results are given in Table I, along with the initial assignments of the individual residues to the active or buffer regions.

Results and Discussion

General Behavior of Atomic Motions. The root mean square fluctuations of atoms relative to their average positions are a measure of the range and time scale of the atomic mobilities. The magnitude of the fluctuations from the simulations may be compared with X-ray experiments (Petsko & Ringe, 1984; Debrunner & Frauenfelder, 1982; Artymiuk et al., 1979); however, care must be exercised in interpreting the measurements (Kuriyan et al., 1986). For a dynamics trajectory of N frames, the rms fluctuation (Δr_{rms}) of an atom is given by

$$(\Delta r_{\mathrm{rms}}) = \left(\frac{1}{N} \sum_{i=1}^{N} |\mathbf{r} - \langle \mathbf{r} \rangle_{\mathrm{av}}|^2 \right)^{1/2} \qquad (2)$$

This may be compared with the temperature factors, B, determined by high-resolution X-ray structure refinement, which are related to the MD rms fluctuations by (Petsko & Ringe)

$$B_i = (8/3)\pi^2 \langle \Delta \mathbf{r} \rangle^2 \qquad (3)$$

This relationship is derived from the Debye–Waller model for harmonic and isotropic motion and further assumes that static lattice disorder is negligible; the assumption of isotropic, harmonic motion has been shown to lead to an underestimation of (Δr_{rms}) when the motion is anharmonic or anisotropic (Kuriyan et al., 1986).

The calculation of different averages of rms fluctuations also provides information regarding the time scale of the fluctuations. Dividing the trajectory into shorter segments and av-

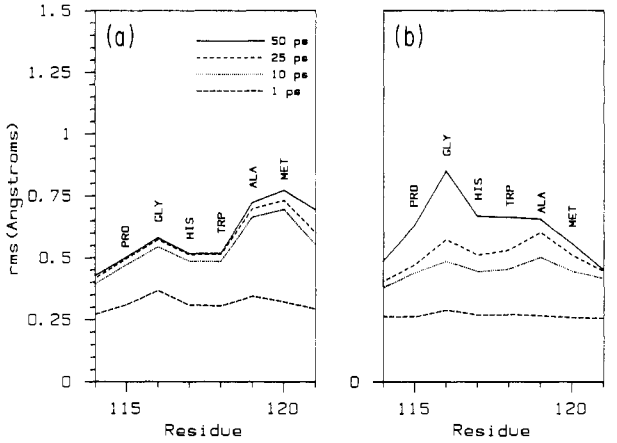

FIGURE 3: Comparison of average rms fluctuations averaged over different time intervals for the backbone atoms of tryptophan 118 and surrounding residues. (a) rms fluctuations averaged over backbone atoms for residues 114–121 for the vacuum simulation (W118V). Convergence is nearly complete at 10 ps. (b) rms fluctuations averaged over backbone atoms for residues 114–121 for the solvent simulations (W118S). Convergence is not reached at 50 ps, indicating motion on this time scale.

eraging the rms values over all segments eliminates contributions from motions slower than the duration of the segment. Comparing the average rms values over different time scales then provides information on the type of motion that gives rise to them (Swaminathan et al., 1982; Post et al., 1986). For each of the three simulation systems, W48, W118S, and W118V, the rms fluctuations for each atom were calculated by using trajectory segment lengths of 1, 10, 25, and 50 ps. These quantities were averaged over each residue, distinguishing backbone and side-chain atoms. (N, C, and C_α atoms were considered backbone atoms; all other atoms including the carbonyl oxygen were considered side-chain atoms.)

The rms averages for most backbone atoms almost converged to their final values when averaged over 10-ps segments. The backbone segment of residues 114–121 in the W118S simulation did not converge, however, over the entire trajectory, indicating that this region in the simulation with solvent experienced motion on a 50-ps or greater time scale (see Figure 3). A glycine residue that shows the largest mobility underwent a dihedral angle transition. As shown in Figure 3a, in the vacuum run, the motions in this region converged in 10 ps. The side-chain rms averages also generally converged in 10 ps, but there were more exceptions. In particular, the side chains of residues 114–121 of W118S, including Trp 118 itself, did not converge; this is in accord with the behavior of the backbone atoms. Several of the side chains of the residues 50–65 in both the solvent (W118S) and vacuum (W118V) simulations did not converge. Also, methionine residues, especially in the vacuum simulation, typically did not converge in 50 ps; this is consistent with the high mobility found for methionine in NMR studies of lysozyme (Olejniczak et al., 1984).

The calculated rms fluctuation values for atoms in the active region are shown in Table II. The interior of the protein (W48) has overall average rms fluctuations of 0.50 Å, smaller than the values of 0.61 and 0.63 Å for the simulations of Trp 118 with (W118S) and without (W118V) solvent, respectively. Both the average side chain and backbone mobilities differ between the interior simulation (W48) and the exterior simulations (W118S and -V). The side chains of the W118 simulations exhibit significantly greater peak mobilities. The rms averages of the side chains are roughly proportional to the corresponding backbone mobilities and are larger in all

Table II: Average rms Fluctuations (Å) for the Atoms in Azurin Ade[a]

atoms	W48	W118V	W118S
backbone	0.40	0.54	0.52
side chain	0.58	0.69	0.67
all	0.50	0.63	0.61

[a] The rms fluctuations are averaged over atoms in the active regions only.

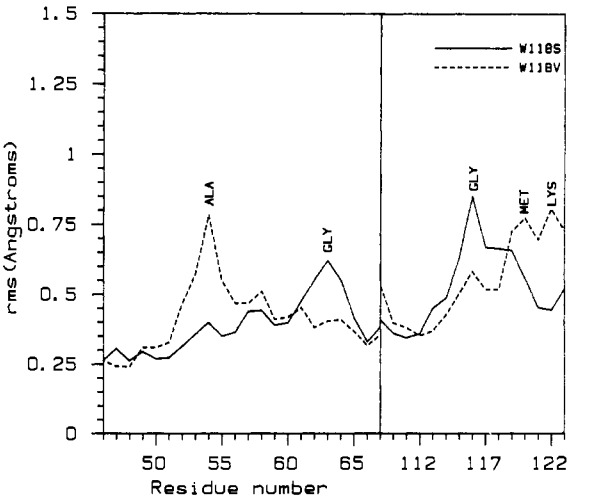

FIGURE 4: Backbone rms fluctuations averaged over 50 ps for two regions of the tryptophan 118 simulations showing solvent effects. The addition of solvent enhances the mobility of several glycine residues and restricts the mobility of other longer side chain residues.

cases. Long side chains have larger rms averages, as might be expected.

The direct comparison of calculated rms mobilities with those determined from the crystallographic temperature factors is complicated by the limitations of the Debye–Waller model, as previously mentioned, by the approximations of the simulation method, and by the fact that many motions may be quite different in crystalline and aqueous environments.

Because of the localized character of the simulation, delocalized librational motions that might contribute significantly to the fluctuations are omitted. The overall magnitudes of the rms fluctuations from the X-ray (0.51 Å) and the simulation (see Table II) are quite similar, and the residue-to-residue variation of the crystallographic averages is reproduced approximately in the simulation. A major qualitative difference between the simulation results and the X-ray results is evident when the backbone and side-chain averages are compared, however. The rms fluctuations from the X-ray data are nearly identical for backbone and side-chain atoms, but the side-chain rms fluctuations are significantly greater for the simulation results. The results of Kuriyan et al. (1986) indicate that anisotropic and anharmonic character of the motions leads to a significant underestimation of the range of side-chain motion in the X-ray analysis, while the backbone results are approximately correct. This may account for much of the discrepancy. It is also possible that the constraints on the backbone atoms due to the use of the stochastic boundary method are more important than those on the side-chain atoms.

Solvent effects may be determined by comparing the two W118 simulations (see Figure 4 and Table II). The presence of solvent does not significantly alter the overall mobilities. Certain side chains that penetrate into the solvent, such as methionine 13, are much more mobile when solvent is not included. Even so, the total average mobilities differ by less than 3%. However, some backbone atoms of high mobility,

such as alanine 54 and methionine 120, have significantly reduced amplitudes in the presence of solvent. Apparently, structured water around side chains restricts their motion and in turn restricts the backbone mobility. On the other hand, the presence of water is seen to actually enhance the mobilities of sections of the backbone centered on glycine residues. One of the regions of increased mobility is the surface segment consisting of residues 114–119, which includes Trp 118. As already mentioned, this is the region in which the motion for W118S has not converged on a 50-ps time scale. It is intriguing that the residue of highest backbone mobility in the W118S simulation (Gly 116) is conserved, along with many of the nearby hydrophobic residues, in all azurins sequenced so far (Norris et al., 1983). Its location in the hydrophobic surface "patch" that has been proposed as the binding surface of the protein, and the fact that it is conserved in the azurin proteins suggests that the flexibility accorded by the glycine is important in binding. One example of the importance of glycine is seen in the conversion of trypsinogen to trypsin, where it has been noted that mobile Gly residues serve as "hinge" for the motion of the activation domains (Brünger et al., 1987).

Motions of Tryptophan. To use tryptophan as a fluorescent probe in experimental studies of protein motion, the relationship between the motions of the indole moiety and the motions of the backbone and protein environment must be understood. Since the experiment measures the reorientation of the transition moments of the indole, it is important to determine the relation of local side-chain fluctuations to larger scale librational motions involving secondary structural elements such as α-helices and β-sheets. It is also of interest to know whether tryptophan motions are strongly correlated with the motions of the immediate environment and whether such correlations have a characteristic propagation distance within the protein matrix.

The azurin protein of *A. denitrificans* contains two tryptophan residues in different environments. Trp 48 is part of a β-strand in the β-barrel in the middle of the molecule; the tryptophan side chain is embedded in the interior of the β-barrel. β-sheets are known to pack tightly against each other in many proteins (Chothia & Lesk, 1982). The compactness of the environment of Trp 48 is expected to restrict the range of its motion. Trp 118 is on the surface of the protein, partially surrounded by hydrophobic residues and partially accessible to solvent molecules; it experiences less restriction on its motion than Trp 48. The Trp 118 backbone is part of a very short pseudohelix, and the indole moiety is in contact with residues of the α-helical segment of the protein (residues 55–67; Norris et al., 1983). We now examine the motions of tryptophan found in the molecular dynamics simulation to investigate the relationship of these motions to protein structure and environment and to assess the usefulness of tryptophan as a probe of protein dynamics.

(*a*) *Atomic Fluctuations.* The autocorrelation functions for tryptophan atom fluctuations were calculated from (Brooks et al., 1985)

$$C_i(t_m) = \frac{1}{N-m}\sum_{n=1}^{N-m}\Delta\mathbf{r}_i(t_n + t_m)\cdot\Delta\mathbf{r}_i(t_n) \qquad (4)$$

which is the molecular dynamics analogue of

$$C_i(t) = \lim_{T\to\infty}\frac{1}{2T}\int_{-T}^{T}\Delta\mathbf{r}_i(t+\tau)\cdot\Delta\mathbf{r}_i(\tau)\,d\tau \qquad (5)$$

where

$$\Delta\mathbf{r}_i = \mathbf{r}_i(t) - \langle\mathbf{r}_i\rangle_{avg} \qquad (6)$$

Table III: Correlation Times of Tryptophan Atom Fluctuations[a]

atom	τ_{W118S} (ps)	τ_{W118V} (ps)	τ_{W48} (ps)
C_α	4.30 (0.67)	0.64 (0.53)	0.33 (0.28)
C_β	4.62 (0.71)	0.67 (0.71)	0.33 (0.31)
C_γ	4.52 (0.67)	0.56 (0.54)	0.34 (0.30)
C_{δ_1}	3.70 (0.72)	0.41 (0.54)	0.27 (0.41)
C_{δ_2}	4.37 (0.67)	0.56 (0.60)	0.27 (0.33)
N_{ϵ_1}	2.00 (0.72)	0.41 (0.55)	0.27 (0.44)
C_{ϵ_2}	3.67 (0.68)	0.49 (0.59)	0.33 (0.37)
C_{ϵ_3}	3.63 (0.71)	0.55 (0.81)	0.27 (0.39)
C_{ζ_2}	1.88 (0.74)	0.47 (0.75)	0.33 (0.44)
C_{ζ_3}	2.80 (0.77)	0.40 (0.98)	0.31 (0.49)
C_{η_2}	1.87 (0.79)	0.41 (0.95)	0.27 (0.49)

[a] The correlation time is defined as the time for $C_i(t)$ to decay to $1/e$ of its initial value; the values in parentheses are rms fluctuations of corresponding atoms (in angstroms).

The number of time points averaged, $N-m$, for the correlation function decreases linearly with time; thus, as t_m gets larger, the calculated $C_i(t_m)$ becomes less accurate, so the correlation function may be calculated only for a fraction of 50 ps (Lee & Karplus, 1984). However, most of the functions have decayed to zero in the first 10 ps and show distinguishing characteristics of the motion.

Several of the tryptophan atom fluctuation correlation functions are shown in Figure 5. The atoms were selected to represent different parts of the residue (see Figure 6). Each function has a smooth, rapid initial decay (0.1 ps) corresponding to inertial motion. For W48 and W118V, the initial rapid decay brings the correlation function close to zero and is followed by an irregular oscillation around zero. The correlation function decays more rapidly in W48 than in W118V. The initial decay in W118S is of smaller amplitude (the correlation function decays to 0.6 of its normalized initial value) and followed by a much slower decay to zero. The correlation times [defined as the time for $C_i(t)$ to decay to $1/e$ of its initial value] for all W48 atoms have small and similar magnitudes (see Table III). For W118V, the τ values are about 50% larger and show a somewhat wider range. Those for W118S are between 5 and 9 times the values for the corresponding atoms in W118V; also, the range of variation is still greater. The rms fluctuations of all tryptophan atoms in the three simulations are also listed in Table III. For W48 and W118V, there is little correlation apparent between the rms fluctuation and the atomic fluctuation correlation time because of the very small range of correlation times. For W118S, there seems to be a small decrease in the magnitude of the rms fluctuation as the correlation time increases.

Steric interactions in the compact protein core lead to steep potential barriers and more collisions with other atoms than for an exposed residue. This has the effect of reducing the magnitude of the rms fluctuation and of shortening the correlation times. This restricted mobility also leads to the similarity of the behavior of all tryptophan atoms, irrespective of their positions on the side chain, as would be expected for the atoms in a compact core region with similar potentials of mean force. The surface tryptophan has a greater range of allowed motion and a somewhat longer correlation time. The much slower decay of the correlation function with the inclusion of solvent is a dynamic effect. Since the rms values show that the range of motion is approximately equivalent in the vacuum and solvent simulations, the motion in the latter is damped due to the interactions with the solvent; i.e., there is a frictional damping that leads to a much slower time development of the fluctuations for both the backbone and the side chains at and near the tryptophan residue (see Figure 3b).

The damping by solvent is also shown by the spectral den-

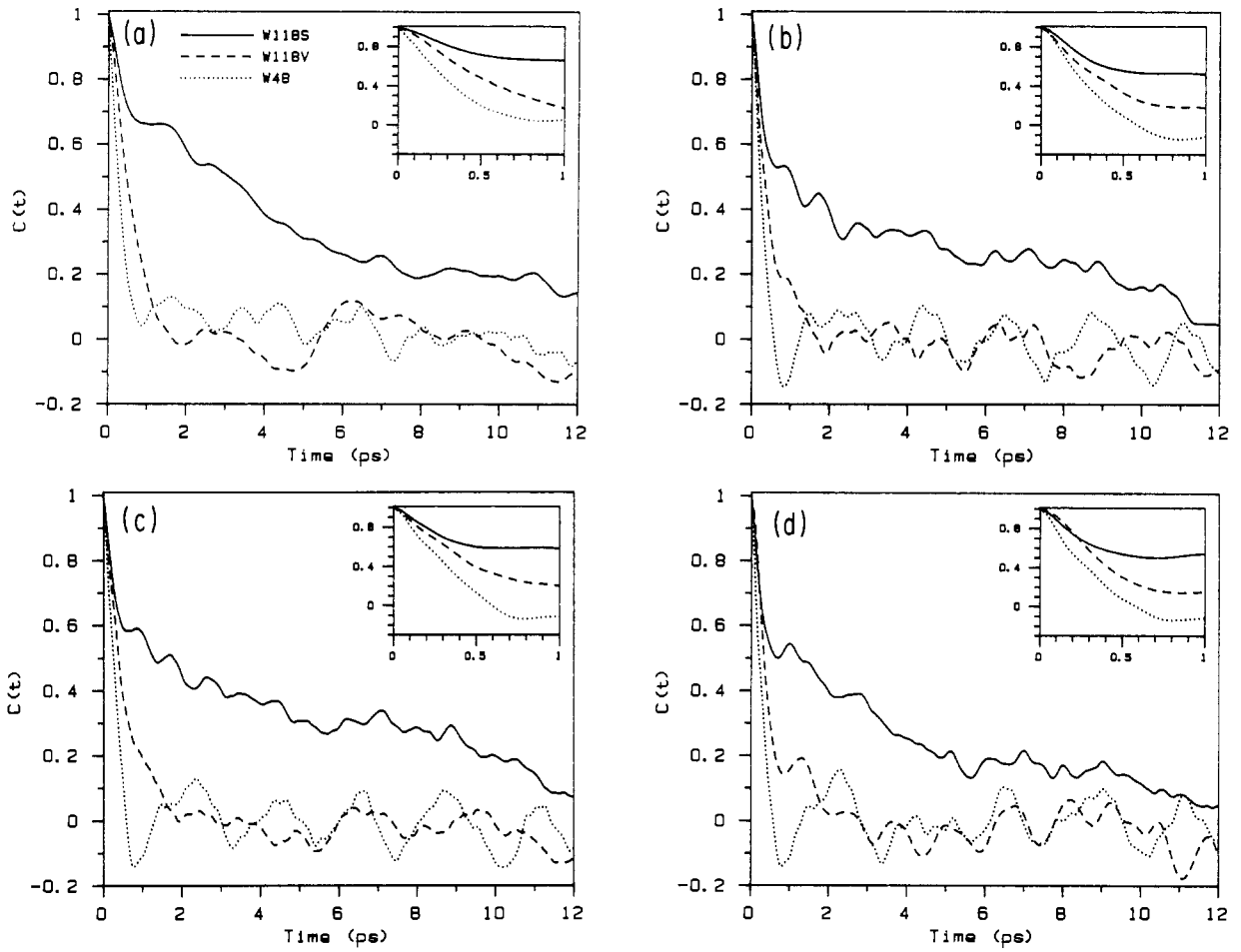

FIGURE 5: Normalized time correlation functions for the fluctuations of tryptophan atoms about their average positions: (a) C_α; (b) N_{ϵ_1}; (c) C_{ζ_2}; (d) C_{ζ_3}. The slower decay of the correlations of W118S (simulation with solvent) is an effect of solvent damping. The inertial behavior of the correlation function is evident at short times (see insert).

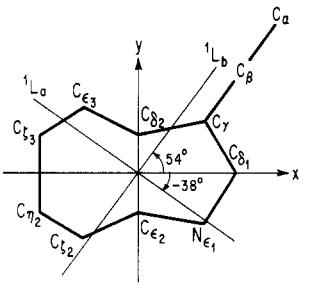

FIGURE 6: Structure of tryptophan. The orientations of the ^1L_a and ^1L_b transition dipoles from Yamamoto and Tanaka (1972) are shown.

sities which characterize the amplitudes of the frequency components of the fluctuations. The spectral density function, $C(\omega)$, is given by

$$C(\omega) = [\Delta \mathbf{r}_i(\omega)]^* \cdot [\Delta \mathbf{r}_i(\omega)] \quad (7)$$

where

$$\Delta \mathbf{r}_i(\omega) = \lim_{T \to \infty} \frac{1}{2T} \int_{-T}^{T} e^{-i\omega t} \Delta \mathbf{r}_i(t)\, dt \quad (8)$$

The results for the three simulations are quite noisy (see Figure 7), making assignments of individual peaks impossible. The most notable feature of the spectral density plots is the very different character of the W118S simulation, which shows a dramatic damping of modes with frequencies higher than approximately 10^{12} Hz.

The finding of increased damping and diffusive motion in the presence of solvent molecules is in accord with the previous studies of van Gunsteren and Karplus (1982), Brooks and Karplus (1986) and Axelsen and Prendergast (1988). These simulations and the present work used essentially identical force fields. In the study of Ahlström et al. (1987), using an independent set of interaction potentials, the presence of solvent speeds up the decay of atomic correlations. In this latter study the vacuum simulation correlation functions decay very slowly and appear to exhibit none of the underdamped motion observed in our simulations.

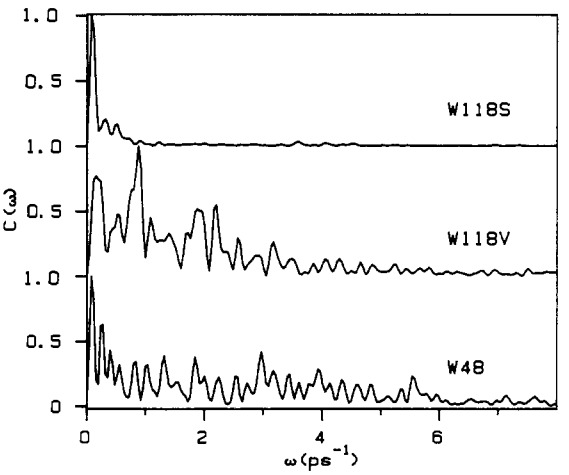

FIGURE 7: Spectral density functions for the three simulations. Solvent damps modes with frequencies higher than approximately 10^{12} Hz in simulation W118S.

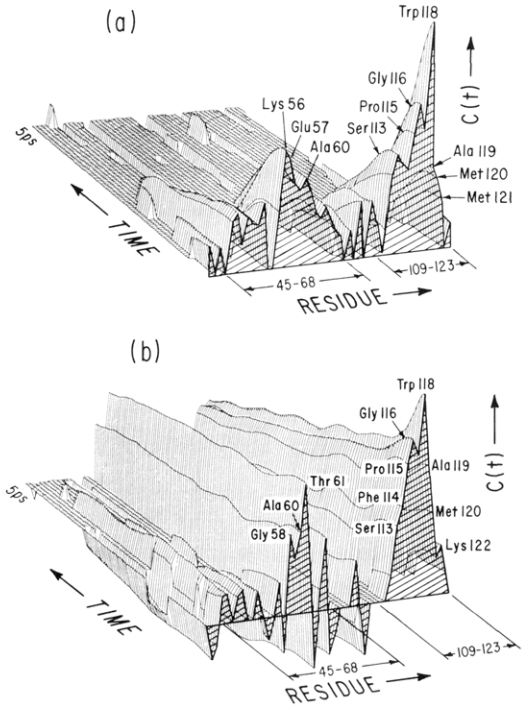

FIGURE 8: Cross-correlation functions of the displacement of residue Trp 118 with the displacements of the other residues in simulation (a) W118V and (b) W118S. The time axis extends for 5 ps, and the vertical scale is identical in both cases. Similar regions have high initial cross correlations with Trp 118 in both simulations, though the sizes of the regions are reduced in W118S. In the presence of solvent, the decay of the correlations is much slower than in vacuum, in accord with the slower fluctuation decay times in simulation W118S.

Table IV: Equal Time Cross Correlations of Trp 118 with Other Residues

residue		C(0)		
no.	type	W118S	W118V	av distance (Å)
		Near Tryptophan 48		
46	His	0.14	0.22	11.60
47	Asn	0.08	0.26	11.07
48	Trp	0.12	0.11	14.19
50	Leu	0.01	0.21	11.52
110	Tyr	−0.04	0.11	13.20
		α-Helix		
56	Lys	0.16	0.51	8.57
57	Glu	−0.19	0.46	6.05
58	Gly	0.39	0.36	9.09
59	Val	0.27	0.32	8.50
60	Ala	0.40	0.38	5.26
61	Thr	0.63	0.32	7.44
62	Asp	0.17	0.22	11.55
63	Gly	−0.29	0.20	10.18
64	Met	0.10	0.25	8.87
65	Asn	0.36	0.20	12.81
66	Ala	−0.23	0.14	14.29
67	Gly	−0.14	0.11	13.67
		Backbone Neighbors		
111	Phe	0.05	0.35	6.74
112	Cys	0.12	0.44	6.37
113	Ser	0.37	0.40	6.27
114	Phe	0.46	0.37	7.58
115	Pro	0.66	0.52	5.34
116	Gly	0.78	0.65	3.72
117	His	0.70	0.54	5.63
118	Trp	1.00	1.00	0.00
119	Ala	0.65	0.37	4.82
120	Met	0.41	0.31	8.03

Atomic fluctuation cross-correlation functions were calculated by

$$C_i'(t_m) = \frac{1}{N-m}\sum_{n=1}^{N-m} \overline{\Delta r_i}(t_n + t_m)\overline{\Delta r_i}'(t_n) \qquad (9)$$

where $\overline{\Delta r_i}$ and $\overline{\Delta r_i}'$ stand for atomic fluctuations that are averaged over residues. We consider the cross correlations between a tryptophan residue and various other residues. Cross-correlation functions for all residues (including the buffer region) were calculated between the average atomic fluctuations of Trp 118 and the average atomic fluctuations of each other residue for simulations W118S and W118V. The results are shown in Figure 8. In each simulation, two regions are highly correlated with tryptophan motions. They are bounded by residues 56–61 and residues 113–120 (both regions are in the active region and are shaded in Figure 1). Equal time cross-correlation values are given in Table IV. The residues in the first region form part of the α-helical segment (comprising residues 55–67) of the molecule and have side chains in close contact with the face of the indole ring of the tryptophan residue. The residues in the second region (including Trp 118) are connected along the backbone, so that large-scale backbone fluctuations are common to each residue in the region. The correlations propagate to approximately 8–9 Å from tryptophan. The magnitudes of the initial correlations of W118S and W118V are approximately equal, but more residues are correlated in the absence of solvent. Without solvent, the entire neighboring α-helix is correlated with the tryptophan motion. The residues on the side of the α-helix nearest to tryptophan have somewhat higher correlations than residues on the other side of the helix. This is shown in Figure 8a as the periodicity of the initial cross-correlation functions in the region of residues 56–62. The addition of solvent alters this significantly. Tryptophan is separated from the α-helix side chains by approximately 5 Å (the shortest distance is 4.0 Å between tryptophan and the alanine 60 side chain). This allows a few water molecules to penetrate between the two parts. In addition, water molecules form a hydrogen bond at the indole nitrogen, which exchanges every few picoseconds. The solvent mediates the correlation with the α-helix, leaving only significant positive correlation with the nearest residues on the α-helix. Other α-helical residues either lose significant correlation or become negatively correlated, such as glutamic acid 57. In both simulations W118V and W118S, the motion of the indole ring of Trp 118 (and thus the transition dipole) reflects the motion of a significant portion of the protein. The correlation with residues close to the face of the indole ring is not surprising; to our knowledge the correlation along the backbone has not been described in previous simulations.

(*b*) *Fluctuations in the Orientation of the Indole Ring.* Tryptophan probes protein environment in several ways. The static or average environment affects the fluorescence properties, so fluorescence spectra and lifetimes serve to indicate the hydrophobicity of the environment or the presence of nearby quenching groups. The dynamical environment is probed by measurement of depolarization due to a variety of motions: overall tumbling, backbone librational modes, or local side-chain fluctuations. Some evidence of dynamic behavior may also be ascertained from fluorescence properties, if, for example, several conformational states can be shown to exist and interconvert with a particular rate. Current models that attempt to explain the multiple-exponential fluorescence decay of tryptophan suggest that the χ_1 and χ_2 dihedral angles determine the fluorescence lifetimes of tryptophan (Donzel et al., 1974; Gauduchon & Wahl, 1970; Fleming et al., 1978; Szabo & Rayner, 1980; Petrich et al., 1983; Chang et al., 1983; Cowgill, 1967; Engh et al., 1986; Tanaka & Mataga, 1987). In particular, it has been proposed that tryptophan fluorescence

is quenched via intramolecular charge transfer from the indole to internal quenchers, e.g., a peptide carbonyl group. The quenching rate is a function of the interaction of the indole ring and the quenching group, which for an individual tryptophan molecule is determined mainly by χ_1 and χ_2 dihedral angles. Different tryptophan conformers (corresponding to different dihedral angles) exhibit different fluorescence lifetimes. Thus, the measured fluorescence lifetimes depend on the fluorescence lifetimes of the individual conformers and the conformer interconversion rate. In the limit of very rapid conformer interconversion, only single-exponential lifetimes should be observed. In a protein environment, nonexponential decays may also arise from differing conformations of the protein matrix itself.

Fluctuations in the χ_1 and χ_2 dihedrals are important in determining the short-time behavior of the fluorescence or absorption anisotropy. On a somewhat longer time scale, lower frequency, more collective modes such as hinging–benching motions or helix reorientations may contribute to the motions of the indole moiety. Because of the general interest in understanding the detailed motions that lead to depolarization of tryptophan and also in understanding how fluctuations may affect fluorescence lifetimes (Tanaka & Mataga, 1987), we analyze in this section the fluctuations of the orientation of the tryptophyl residues. We focus on the fluctuations and transitions involving χ_1 and χ_2 dihedral angles and on the reorientation of indole transition dipole moments (Ichiye & Karplus, 1983).

The mobility of a tryptophyl residue in a protein may be determined by time-resolved fluorescence depolarization experiments. The rotational correlation function $r(t)$ measured in an idealized experiment is given by

$$r(t) = \frac{i_{\parallel}(t) - i_{\perp}(t)}{i_{\parallel}(t) + 2i_{\perp}(t)} \tag{10}$$

where $i_{\parallel}(t)$ and $i_{\perp}(t)$ are the fluorescence intensities polarized parallel and perpendicular to the excitation polarization, respectively. $r(t)$ is related to the orientation of the absorption and emission transition dipole moments by (Levy & Szabo, 1982)

$$r(t) = \tfrac{2}{5}\langle P_2[\mu_a(0)\cdot\mu_e(t)]\rangle \tag{11}$$

where P_2 denotes the second Legendre polynomial; μ_a and μ_e are unit vectors in the absorption and emission dipole directions, respectively, and the broken brackets denote an ensemble averaging. In many cases involving globular proteins, this function is represented well by a sum of two exponential terms (Lipari & Szabo, 1982; Ichiye & Karplus, 1983)

$$\left[\frac{r(t)}{r(0)}\right] \approx A_\infty \exp(-t/\tau_M) + (1 - A_\infty)\exp[-t(\tau_M^{-1} + \tau_{eff}^{-1})] \tag{12}$$

where a longer decay time τ_M is associated with overall molecular tumbling and a shorter decay time τ_{eff} corresponds to the restricted internal motion. The restricted internal motion will not reduce the anisotropy to zero but to a plateau value defined as A_∞. The time resolution for such experiments using current technology ranges from about 0.2 ps for pump-probe techniques (Fleming, 1986) to 10–20 ps for single photon counting. Petrich et al. (1987) measured the fluorescence anisotropy for the apoazurins from *Pseudomonas aeruginosa* (Pae) and *Alcaligenes faecalis* (Afe) with time resolution of 40–50 ps. Azurin Pae contains only a single, interior tryptophan (Ambler, 1973), and its fluorescence anisotropy was single exponential with a time constant of 5 ns, corresponding to overall molecular tumbling (Petrich et al., 1987). Azurin Afe, containing only the exposed tryptophan (Ambler, 1973), had a biexponential anisotropy, with a short-time decay of 160 ps accompanied by a long-time component of 7 ns (Petrich et al., 1987). The 7-ns component was again assigned to overall tumbling, and the fast-decay component was attributed to restricted internal motion of the tryptophan residue. These results indicate that surface tryptophan has substantially greater mobility than interior tryptophan.

Table V: χ_1, χ_2 Trajectory Statistics (in Degrees)

	W48	W118S	W118V	W118V[a] (35 ps)
$\langle\Delta\chi_1\rangle_{rms}$[b]	6.52	8.29	13.34	22.91
$\langle\Delta\chi_2\rangle_{rms}$[b]	10.54	8.93	20.52	25.77
$\langle\Delta\chi_1(0)\Delta\chi_2(0)\rangle$[c]	−0.06	0.17	−0.76	−0.61

[a] See figure caption for Figure 10. [b] Calculated by eq (2), x is substituted by χ_1 or χ_2. [c] Calculated by eq (9), r is substituted by χ_1 or χ_2.

Equation 12 is an approximation that may not be valid for certain kinds of restricted motion for which the short-time decay may not be simply exponential. For these cases the extent of motion may be characterized by the model-independent order parameter S (Lipari & Szabo, 1982; Chang et al., 1983b)

$$S^2 = \lim_{t\to 0^+} \frac{r(t)}{r(0)} e^{t/\tau_r} = \frac{r(0^+)}{r_{eff}(0)} \tag{13}$$

where τ_r is the overall tumbling time, $r_{eff}(0)$ is the actual value of the initial anisotropy (which may not be 0.4), and $r(0^+)$ is the value of the initial anisotropy obtained by extrapolation of the long-time (tumbling) behavior. Thus, for the case that $S^2 = 1$, the chromophore is held rigid in the molecular frame; values less than unity indicate flexibility. If the restricted motion is modeled as free rotation within a cone with a semiangle of θ_0, S becomes (Lipari & Szabo, 1980)

$$S = \tfrac{1}{2}\cos\theta_0(1 + \cos\theta_0) \tag{14}$$

Using this analysis, Petrich et al. (1987) obtained a semiangle in the range of 26–38° for the restricted motion of the surface tryptophan of azurin Afe. For the buried tryptophan of azurin Pae, the lack of a detectable short component in the anisotropy implies a semiangle of $\leq 20°$.

The time series of χ_1 and χ_2 for the three systems are plotted in Figure 9. The magnitudes of the fluctuations of χ_1 and χ_2 are given in Table V. The fluctuations of W118S and W48 have approximately the same amplitude, and as for atomic fluctuation, both show high-frequency fluctuations. However, the χ_1 and χ_2 time series of W118S appear to show a slow fluctuation (with approximately 10-ps period) in addition to the fast local fluctuation. No χ_1 or χ_2 transitions were observed in either of these two simulations. Omission of solvent (W118V) led to significantly greater χ_1 and χ_2 fluctuations. Two transitions of each dihedral angle were also observed (see Figure 9). An additional 10 ps for each simulation duplicated these results, with no transitions observed for W48 and W118S but an additional χ_1 and χ_2 transition for W118V. A notable feature of the simulations is the strong anticorrelation that exists between the two dihedral angles in W118V (see Figure 10). This anticorrelation was less evident in previous simulations of an individual tryptophan (Engh et al., 1986) but was noted in the lysozyme tryptophan motions (Ichiye & Karplus, 1983). The greater steric restriction around the tryptophan in the protein appears to be the origin of coordinated transitions. It is interesting that in solvent there is a positive correlation between χ_1 and χ_2. Although no χ_1 or χ_2 tran-

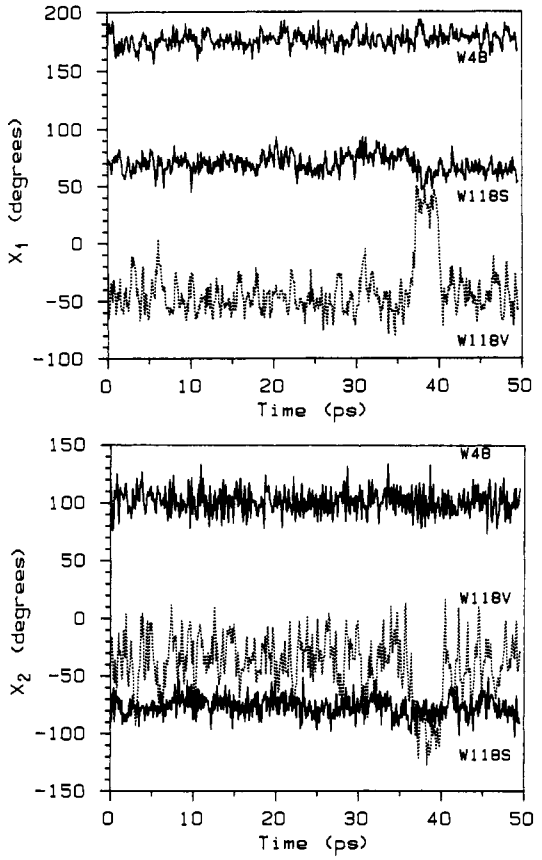

FIGURE 9: Trajectories of the χ_1 and χ_2 dihedral angles for the three simulations. Transitions are seen in the simulation of tryptophan 118 without solvent (W118V), which are also seen in the following 10-ps trajectory (not shown). Addition of solvent (W118S) hinders the transitions (in this time period) and introduces a slow fluctuation with a period of approximately 10 ps.

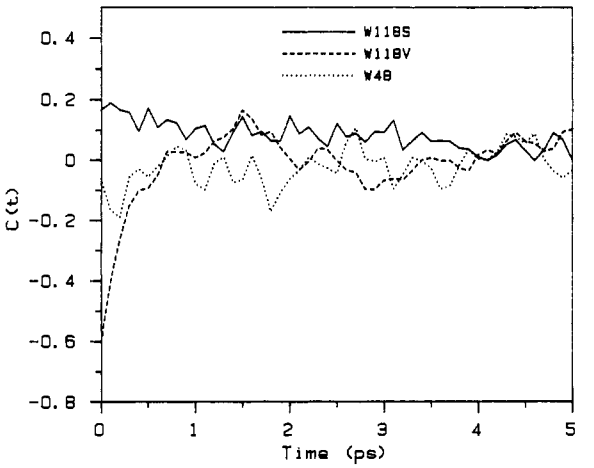

FIGURE 10: Cross-correlation functions of the fluctuations of χ_1 and χ_2 dihedrals about their average values. The functions were calculated over the 50-ps trajectories for W48 and W118S; 35 ps was used for W118V to avoid distortions arising from the χ_1 and χ_2 transitions. The dihedral fluctuations are strongly anticorrelated in the absence of solvent (W118V); this correlation disappears with the introduction of solvent. The decay of the correlation is approximately equal to the decay of the autocorrelations of the dihedral fluctuations. Calculating the cross-correlation functions for W118V over 50 ps, thereby introducing the region of dihedral transitions that are clearly anticorrelated, enhances the initial correlation value to −0.75 and increases the lifetime of the cross correlation.

sitions were observed in the W118S or W48 simulations, the fact that they occurred in the W118V simulation indicates that the protein itself does not prevent them. It is likely that the presence of solvent decreases the probability of occurrence so that none were observed during the trajectory. If this is true, χ_1 and χ_2 conformers might still play an important role in energy- and electron-transfer processes in solvated protein. Solvent may also alter the relative energies of the different conformations; a much longer dynamics simulation or alternative simulation methods (e.g., umbrella sampling) would be required to clarify this point.

To compare the simulation results with fluorescence anisotropy measurements, the anisotropy was calculated by using (Ichiye & Karplus, 1983)

$$\langle P_2[\mu_a(0)\cdot\mu_e(t_m)]\rangle \approx (N-m)^{-1}\sum_{n=1}^{N-m} P_2[\mu_a(t_n)\cdot\mu_e(t_n+t_m)] \quad (15)$$

where μ_a and μ_e are the absorption and emission transition dipoles of tryptophan in the molecule fixed frame. The calculated anisotropy refers only to internal motions. It has been observed that the long wavelength absorption band of tryptophan consists of two electronic transitions, ^1L_a and ^1L_b (Konev, 1967; Song & Kurtin, 1969; Andrews & Foster, 1974). The orientations of these transition dipole moments are at a large angle with respect to each other (Yamamoto & Tanaka, 1972). Several studies have determined the orientations of related ^1L_a and ^1L_b transition dipole moments in indole derivatives other than tryptophan (Callis, 1984; Negus, 1985; Philips & Levy, 1986). The orientations vary slightly in the different compounds. It has also been suggested that the absorption and emission dipoles are not parallel (Sun & Song, 1977). For our purposes, we assume the orientations of the transition dipoles for the ^1L_a and ^1L_b transitions to be those determined by Yamamoto and Tanaka for indole (Yamamoto & Tanaka, 1972; also see Figure 6), namely, −38° and +54° from the long axis of indole, respectively, and that μ_e is parallel with μ_a. The calculated $P_2(t)$ results for ^1L_a excitation and emission and ^1L_b excitation and emission for the three tryptophan simulations are shown in Figure 11. Each system shows a very rapid initial decay to an anisotropy that is nearly constant on the time scale of the simulation. The difference between the initial anisotropy and this plateau value is an indication of the range of motion available to the transition dipole, and the value of the plateau corresponds to S^2 on a picosecond time scale. For W48, W118S, and W118V, respectively, the values of 0.94, 0.91, and 0.86 correspond to semiangles of the cone model of 16°, 20°, and 25° for the ^1L_a transition dipole, and the values of 0.96, 0.93, and 0.89 correspond to θ_0 of 9°, 13°, and 16° for the ^1L_b transition dipole. In accord with the analysis of the other motional properties of the tryptophans, flexibility is increased at the protein surface (relative to the interior) and is decreased by solvent (relative to vacuum). Further, for the two realistic simulations (W48 and W118S), the picosecond-order parameter and cone semiangle are quite similar to the experimental measurements (see above). It is difficult to assess the significance of this similarity because no long-time component corresponding to the measured 160 ps for the exterior tryptophan is observed in the simulation. In other words, although the extent of the motion is roughly correct, the time scale is not. It is not surprising, given the length of the simulations, that a slower decay is not observed. It is also possible that the 160-ps component is due to a librational mode involving large portions of the molecule. The stochastic boundary method would not be able to reproduce this. It is more likely that χ_1 and χ_2 transitions occurring on a 100–200-ps time scale give rise to the decay; a much longer simulation would be required to confirm this.

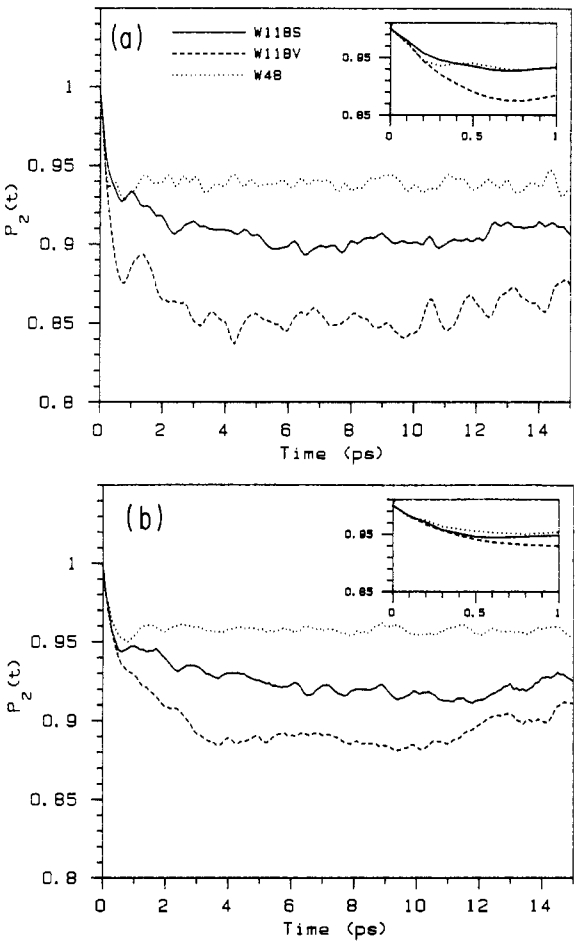

FIGURE 11: Correlation functions $\langle P_2[\mu_a(0)\cdot\mu_e(t)]\rangle$ for (a) ^1L_a and (b) ^1L_b transition dipoles of tryptophan for the three systems. The functions decay to a plateau value corresponding to the range of motion available to the tryptophan residues. Tryptophan 48 is the most restricted, and tryptophan 118 without solvent is least restricted.

(*c*) *Energy Transfer.* Petrich et al. (1987) measured the fluorescence lifetime of the tryptophan in azurin Ade at 355 nm using the single photon counting method. The lifetime was fit to a function of two decaying exponentials and one increasing exponential with a rise time of 1 ns. This 1-ns component was attributed to energy transfer from Trp 48 to Trp 118. The interior Trp 48 of azurin Ade has a very blue-shifted emission maximum at 308 nm that enables energy transfer from Trp 48 to the exposed Trp 118. Petrich (1985) further estimated the energy-transfer rate on the basis of the X-ray structure of azurin. As indicated in the analysis, the neglect of dynamic effects on energy-transfer rate estimates can lead to significant error (Stryer et al., 1982; Somogyi et al., 1984) since the results are sensitive to the relative orientation and the distance of the chromophores. In fact, if the average, static structure happens to have a very low transfer probability due to unfavorable orientations, slight fluctuations in orientation can lead to a significant increase in the transfer probability. Furthermore, the inverse sixth power dependence of energy transfer on separation implies that significant variation in donor–acceptor distance has an important effect on the transfer rates. In this section we present an analysis of the effects of the simulated azurin dynamics on estimated energy-transfer rates.

In the azurin crystal structure, the tryptophan residues are separated by an average distance of 13 Å. At this distance, there should be no significant overlap of donor and acceptor wave functions. Thus, energy transfer between Trp 48 and Trp 118 may be considered in the weak coupling limit, which treats the transfer as due to dipole–dipole coupling. Förster (1959) expressed the energy-transfer rate via the Golden Rule as

$$k_{ET} = \frac{3}{2}\kappa^2\frac{1}{\tau_D}\left(\frac{R_0}{R}\right)^6 \tag{16}$$

Here κ^2 is the orientation factor for the dipole–dipole interaction given by

$$\kappa = \mu_D\cdot\mu_A - 3(\mu_D\cdot\mathbf{r})(\mu_A\cdot\mathbf{r}) \tag{17}$$

where μ_D and μ_A are unit vectors in the direction of the transition dipole moments of the donor and the acceptor, respectively, and $\mathbf{r}$ is the unit vector in the direction of the displacement of the donor and the acceptor. κ varies from −2 to 2. τ_D is the fluorescence lifetime of the donor in the absence of the acceptor, R is the separation between the donor and the acceptor, and R_0 is a critical transfer distance given by

$$R_0^6 = \frac{9000(\ln 10)\phi_D(2/3)}{128\pi^5 n^4 N}\int_0^\infty F_D(\bar{\nu})\epsilon_A(\bar{\nu})\frac{d\bar{\nu}}{\bar{\nu}^4} \tag{18}$$

ϕ_D is the fluorescence quantum yield of the donor in the absence of the acceptor, n is the refractive index of the medium, N is Avogadro's number, $F_D(\bar{\nu})$ is the fluorescence intensity of the donor as a function of frequency ν normalized to unit area, and $\epsilon_A(\bar{\nu})$ is the molar extinction coefficient of the acceptor.

Experimental measurements of Trp–Trp energy transfer involve averages over large ensembles of molecules. To compare these results directly with those from simulations, it would be necessary to simulate the entire protein and the surrounding solvent molecules for a time long enough to sample all possible structural fluctuations with statistically significant frequencies. Computational constraints make this impractical; however, it is possible to make some estimates of the effects of the internal motions on energy-transfer rates from our SBMD simulations. Since the two tryptophan residues were treated in separate simulations, it is necessary to assume for the purpose of this analysis that a fluctuation in W48 is uncorrelated with a fluctuation in W118S. The low cross correlations between Trp 118 and the residues in the neighborhood of Trp 48 (Table IV) support this assumption. To estimate the energy-transfer rate in solvated azurin, we averaged the rate equation over the 1000 × 1000 pairs of configurations from each 50-ps trajectory.

Since κ^2 and R are the only variables in the ensemble, averaging over κ^2/R^6 is equivalent to averaging over k_{ET}. To determine the effects of the dynamics, we compared two ways of calculating the average of κ^2/R^6. In method 1, we determined the time-averaged structure from which the average values of κ and R were determined. These average values were then used to calculate an average orientation factor, $\bar{\kappa}^2$ and the average of the magnitude of the vector connecting the two transition dipoles, $\bar{R}$. In method 2, a dynamical average is calculated. This is done by computing the quantity κ^2/R^6 for each pair of configurations. This average is defined by

$$\left(\frac{\kappa^2}{R^6}\right)_{dyn} = \frac{1}{n^2}\sum_{i=1}^{n}\sum_{j=1}^{n}\frac{\kappa^2(\{\mathbf{r}_i\},\{\mathbf{r}_j\})}{R^6(\{\mathbf{r}_i\},\{\mathbf{r}_j\})} \tag{19}$$

where n is the number of time points in the simulation and $\{\mathbf{r}_i\}$ is a vector of atomic coordinates for a particular configuration. Since both excited states, ^1L_a and ^1L_b, are potentially involved in the energy transfer, the two averages were determined for each possible ^1L_a, ^1L_b combination. We assume,

Table VI: Energy-Transfer Averages

system	quantity	$L_a \rightarrow L_a$	$L_b \rightarrow L_b$	$L_a \rightarrow L_b$	$L_b \rightarrow L_a$
X-ray	κ^2	0.605	1.824	0.362	0.359
	$R(A)$	15.36	15.36	15.36	15.36
	κ^2/R^6 ($10^8 A^{-6}$)	4.605	13.89	2.757	2.734
W118V	κ^2	0.120	0.103	0.645	2.030
(method 1)	$R(A)$	14.79	14.79	14.79	14.79
	κ^2/R^6 ($10^8 A^{-6}$)	1.142	1.125	6.159	19.40
W118V	κ^2	0.136	0.140	0.637	1.942
(method 2;	$R(A)$	14.81	14.81	14.81	14.81
dynamic)	$\overline{(\kappa^2/R^6)}$ ($10^8 A^{-6}$)	1.291	1.325	6.038	18.40
W118S	κ^2	0.134	1.711	0.172	0.144
(method 1)	$R(A)$	15.56	15.56	15.56	15.56
	κ^2/R^6 ($10^8 A^{-6}$)	0.941	12.06	1.214	1.015
W118S	κ^2	0.157	1.664	0.205	0.177
(method 2;	$R(A)$	15.59	15.59	15.59	15.59
dynamic)	$\overline{(\kappa^2/R^6)}$ ($10^8 A^{-6}$)	1.096	11.59	1.429	1.231

as stated previously, that the absorption and emission transition dipole moments in a given state are parallel and that the transition dipoles for ^1L_a and ^1L_b are oriented at −38° and +54° with respect to the long axis of indole, respectively.

The results from these two methods, as well as the value of κ^2/R^6 calculated from X-ray structure, are shown in Table VI. Comparison of the appropriate averages reveals a variety of effects. To determine the effect of dynamics, a comparison of the dynamically averaged κ^2/R^6 (method 2) with the κ^2/R^6 value calculated from the average structure (method 1) is required. Conformational changes between the X-ray structure and the simulation structure alter the energy-transfer parameters significantly. For example, referring to $^1L_b \rightarrow {}^1L_b$ transfer for the W118V simulation the orientation factor calculated from the average structure is 0.103, but the orientation factor is 1.8 in the X-ray structure. Structural differences are smaller between the solvent simulation (W118S) and the X-ray structure but are still significant for the energy-transfer parameters. The influence of dynamics is mainly on the orientation factor; on the time scale of our simulation, the variation of R can be neglected. For example, again for $^1L_b \rightarrow {}^1L_b$ transfer, method 1 gives $\kappa^2 = 0.103$, whereas method 2 gives $\kappa^2 = 0.140$ in the W118V case. The influence of dynamics is to reduce large static orientation factors and to increase small orientation factors.

In order to compare with the experiment we need an experimental value for the overlap integral and donor quantum yield in eq 18 and the donor fluorescence lifetime in eq 16. According to Petrich (1985) the overlap integral is 3.0×10^{16} cm^6 mol^{-1}, $\phi_D = 0.37$ (Szabo et al., 1983), and $\tau_D = 5.16$ ns. Given these values the energy-transfer times corresponding to the various entries in Table VI range from 17.6 to 0.92 ns, as compared with the experimental value of about 1 ns (Petrich, 1985). The X-ray structure and solvated simulation favor the $^1L_b \rightarrow {}^1L_b$ transition. Because of the large change in orientation in W118V, the κ^2 value for $^1L_b \rightarrow {}^1L_b$ transfer is now very small. However, there is now a large value of κ^2 for $^1L_b \rightarrow {}^1L_a$ transfer, and a similar energy-transfer rate is predicted for this transition. Because of the hydrophobic environment of W48 the donor state is expected to be the ^1L_b level. It is encouraging that rates very similar to the experimental value are obtained from this initial level in the simulations. Absolute comparison with experiment is not simple even if the W48 emission spectrum is that of pure ^1L_b since the absorption band of W118 presumably contains overlapping contributions of ^1L_a and ^1L_b states, and the overlap integral should be decomposed into its two contributions before the rates are calculated. In the numerical estimates given above it is assumed that the entire overlap integral contributes to the transition in question and that therefore these rates must be taken as upper limits. Dynamics seems to play a rather minor role, at least on the time scale of our simulations, with the maximum increases and decreases in rate being about ±20%.

Conclusion

The simulations are in qualitative accord with the experimental finding (Petrich et al., 1987) that the interior tryptophan (W48) is less mobile than the exterior tryptophan (W118) in azurin Ade.

The 50-ps simulated tryptophan fluorescence anisotropy decays did not reveal a slowly decaying component for W118 (~160 ps) found experimentally. It is possible that this decay comes from χ_1 and χ_2 transitions on a 100–200-ps time scale; longer simulations or special methods will be required to reproduce the experimental results. The small, rapid (~0.5 ps) drops in anisotropy found in the simulations would not be observable at the time resolution or accuracy of the available measurements.

The inclusion of TIP3P "water" as solvent had a large effect on the time scale of the motion of W118 but not on the magnitude of the rms fluctuations of atomic positions. The solvent damps motions with a frequency greater than 10^{12} Hz and significantly retards the decay of correlations of atom fluctuations. This indicates that of the two possible effects of the solvent i.e., change in potential of mean force and frictional damping [see Brooks and Karplus (1986)], the latter is much more important than the former in the present case. Further, the time scale of the solvent damping corresponds to the rotational correlation time of water molecules.

All three simulations, in accord with previous results, show that the amino acid side chains have higher mobility than the backbones. rms fluctuations derived from X-ray data are of similar magnitude to the simulated values. However, the X-ray temperature factors do not indicate a significant difference between side-chain and backbone atoms. Possible sources for this difference are discussed.

In simulations both with and without solvent the motion of W118 is strongly correlated with the motions of residues connected along the backbone and residues close to the face of the indole ring. Without solvent, the correlation persists through the entire α-helix facing the tryptophan; with solvent, the correlation is restricted to the nearest residues in the α-helix. The distance range over which tryptophan motion is correlated with other residues is roughly 8–9 Å. This suggests that time-resolved anisotropy measurements on tryptophan residues do probe motion of a substantial portion of the protein.

Transition between χ_1 and χ_2 conformers of Trp 118 was observed in the vacuum simulation. No transitions were observed in the simulations with solvent or for W48. However, the W118V results show that the protein itself does not prevent conformer interconversion and that different conformers may play a role in the photophysical behavior of tryptophan residues in proteins.

Estimates of energy transfer between Trp 48 and Trp 118 give rates quite similar to the experimental value, provided the initial state is ^1L_b. The solvated simulation and X-ray structures suggest that the rate is dominated by the $^1L_b \rightarrow {}^1L_b$ transition, whereas the conformation changes occurring in the vacuum simulation favor the $^1L_b \rightarrow {}^1L_a$ transition. The influence of dynamics on the rate is quite minor with changes

in calculated rates of ±20% resulting from the motion.

In summary, the present simulations support the use of tryptophan as a probe of protein mobility, show the crucial importance of solvent in determining time scales (but not the magnitudes) of the motion, and point out the need for improvements in both experiment and theory.

ACKNOWLEDGMENTS

We thank Dr. Stanley Watowich for assistance with the Lesk and Hardman graphics software, Professor Jim Longworth for providing some useful suggestions, and Dr. Jacob Petrich for kindly offering his experimental results and comments on the work.

Registry No. Water, 7732-18-5.

REFERENCES

Ahlstrom, P., Teleman, O., Jonsson, B., & Forsen, S. (1987) *J. Am. Chem. Soc. 109*, 1541.

Ambler, R. P. (1973) in *Recent Developments in Chemical Study of Protein Structures* (Coletti-Previero, M. A., Ed.) pp 289–305, INSERM, Paris.

Andrews, L. J., & Forster, L. S. (1974) *Photochem. Photobiol. 19*, 353.

Artymiuk, P. J., Blake, C., Grace, D., Oatley, S., Phillips, D. C., & Sternberg, M. (1979) *Nature (London) 280*, 563.

Axelsen, P. H., & Prendergast, F. G. (submitted for publication in *Biochemistry*).

Bernstein, F. C., Koetzle, T. F., Williams, G. J. B., Meyer, E. F., Jr., Brice, M. D., Rodgers, J. R., Kennard, O., Shimanouchi, T., & Tasumi, M. (1977) *J. Mol. Biol. 112*, 535.

Brooks, B. R., Bruccoleri, R. E., Olafson, B. D., States, D. J., Sweminathan, S., & Karplus, M. (1983) *J. Comput. Chem. 4*, 187.

Brooks, C. L., III, & Karplus, M. (1983) *J. Chem. Phys. 79*, 6312.

Brooks, C. L., III, & Karplus, M. (1986) *Methods Enzymol. 127*, 369.

Brooks, C. L., III, Brunger, A. T., & Karplus, M. (1985) *Biopolymers 24*, 843.

Brunger, A. T., Brooks, C. L., III, & Karplus, M. (1984) *Chem. Phys. Lett. 105*, 495.

Brunger, A. T., Huber, R., & Karplus, M. (1987) *Biochemistry 26*, 5153.

Callis, P. R. (1984) *Int. J. Quantum Chem. 18*, 579.

Chang, M. C., Petrich, J. W., McDonald, D. B., & Fleming, G. R. (1983a) *J. Am. Chem. Soc. 105*, 3818.

Chang, M. C., Cross, A. J., & Fleming, G. R. (1983b) *J. Biomol. Struct. Dyn. 1*, 299.

Chothia, C., & Lesk, A. M. (1982) *J. Mol. Biol. 160*, 309.

Cowgill, R. W. (1967) *Biochim. Biophys. Acta 133*, 6.

Creed, D. (1984) *Photochem. Photobiol. 39*, 537.

Debrunner, P. G., & Frauenfelder, H. (1982) *Annu. Rev. Phys. Chem. 33*, 283.

Demchenko, A. P. (1986) *Ultraviolet Spectroscopy of Proteins*, pp 5–221, Springer-Verlag, Berlin.

Dobson, C. M., & Karplus, M. (1986) *Methods Enzymol. 131*, 362.

Donzel, B., Gauduchon, P., & Wahl, Ph. (1974) *J. Am. Chem. Soc. 96*, 801.

Engh, R. A., Chen, L. X.-Q., & Fleming, G. R. (1986) *Chem. Phys. Lett. 126*, 365.

Finazzi-Agro, A., Giovagnoli, C., Avigliano, L., Guerrieri, P., Boffi, V., & Mondovi, B. (1970) *Biochemistry 9*, 2009.

Finazzi-Agro, A., Giovagnoli, C., Avigliano, L., Rotilio, G., & Modovi, B. (1973) *Eur. J. Biochem. 34*, 20.

Fleming, G. R. (1986) *Chemical Applications of Ultrafast Spectroscopy*, Oxford University, New York.

Fleming, G. R., Morris, J. M., Robbins, R. J., Woolfe, G. J., Thistlethwaite, P. J., & Robinson, G. W. (1978) *Proc. Natl. Acad. Sci. U.S.A. 75*, 4652.

Fletcher, R., & Reeves, C. M. (1964) *Comput. J. 7*, 149.

Forster, Th. (1959) *Discuss. Faraday Soc. 27*, 7.

Gall, C. M., DeVerdi, J. A., & Opella, S. J. (1981) *J. Am. Chem. Soc. 103*, 5039.

Gall, C. M., Cross, T. A., DeVerdi, J. A., & Opella, S. J. (1982) *Proc. Natl. Acad. Sci. U.S.A. 79*, 101.

Gauduchon, P., & Wahl, Ph. (1970) *Biochemistry 9*, 87.

Gurd, F. R. N., & Rothgeb, T. M. (1979) *Adv. Protein Chem. 33*, 73.

Henry, E. R., Levitt, M., & Eaton, W. A. (1985) *Proc. Natl. Acad. Sci. U.S.A. 82*, 2034.

Henry, E. R., Eaton, W. A., & Hochstrasser, R. M. (1986) *Proc. Natl. Acad. Sci. U.S.A. 83*, 8982.

Hochstrasser, R. M., & Negus, D. K. (1984) *Proc. Natl. Acad. Sci. U.S.A. 81*, 4399.

Ichiya, T., & Karplus, M. (1983) *Biochemistry 22*, 2884.

Jorgensen, W. L. (1981) *J. Chem. Phys. 103*, 335.

Karplus, M., & McCammon, J. A. (1981) *CRC Crit. Rev. Biochem. 9*, 243.

Karplus, M., & McCammon, J. A. (1983) *Annu. Rev. Biochem. 53*, 263.

Konev, S. V. (1967) *Fluorescence and Phosphorescence of Proteins and Nucleic Acids*, Plenum, New York.

Kuriyan, J., Petsko, G. A., Levy, R. M., & Karplus, M. (1986) *J. Mol. Biol. 190*, 227.

Lakowicz, J. R., Maliwal, B. P., Cherek, H., & Balter, A. (1983) *Biochemistry 22*, 1741.

Lee, S., & Karplus, M. (1984) *J. Chem. Phys. 81*, 6106.

Lesk, A. M., & Hardman, K. D. (1982) *Science (Washington, D.C.) 216*, 539.

Levy, R. M., & Szabo, A. (1982) *J. Am. Chem. Soc. 104*, 2073.

Lipari, G., & Szabo, A. (1980) *Biophys. J. 30*, 489.

Lipari, G., & Szabo, A. (1982) *J. Am. Chem. Soc. 104*, 4559.

Longworth, J. W. (1971) in *Excited States of Proteins and Nucleic Acids* (Weinryb, I., Ed.) p 319, Plenum, New York.

Munro, I., Pecht, I., & Stryer, L. (1979) *Proc. Natl. Acad. Sci. U.S.A. 76*, 56.

Negus, D. K. (1985) Ph.D. Thesis, University of Pennsylvania.

Norris, G. A., Anderson, B. F., & Baker, E. N. (1983) *J. Mol. Biol. 165*, 501.

Olejniczak, E. T., Dobson, C. M., & Levy, R. M. (1984) *J. Am. Chem. Soc. 106*, 1923.

Petrich, J. W. (1985) Ph.D. Thesis, The University of Chicago.

Petrich, J. W., Chang, M. C., McDonald, D. B., & Fleming, G. R. (1983) *J. Am. Chem. Soc. 105*, 3824.

Petrich, J. W., Longworth, J. W., & Fleming, G. R. (1987) *Biochemistry 26*, 2711.

Petsko, G. A., & Ringe, D. (1984) *Annu. Rev. Biophys. Bioeng. 13*, 331.

Philips, L. A., & Levy, D. H. (1986) *J. Phys. Chem. 90*, 4921.

Post, C. B., Brooks, B. R., Karplus, M., Dobson, C. M., Artymiuk, P. J., Cheetham, J. C., & Phillips, D. C. (1986) *J. Mol. Biol. 190*, 455.

Rice, D. M., Wittebort, R. J., Griffin, R. G., Meirovitch, E., Stimson, E. R., Meinwold, Y. C., Freed, J. H., & Scheraga, H. A. (1981) *J. Am. Chem. Soc. 103*, 7707.
Richarz, R., Nagayama, K., & Wüthrich, K. (1980) *Biochemistry 19*, 5189.
Somogyi, B., Matko, J., Papp, S., Hevessy, J., Welch, G. R., & Damjanovich, S. (1984) *Biochemistry 23*, 3403.
Song, P.-S., & Kurtin, W. E. (1969) *J. Am. Chem. Soc. 91*, 4892.
Stryer, L., Thomas, D. D., & Mears, C. F. (1982) *Annu. Rev. Biophys. Bioeng. 11*, 203.
Sun, M., & Song, P.-S. (1977) *Photochem. Photobiol. 25*, 3.
Szabo, A. G., & Rayner, D. M. (1980) *J. Am. Chem. Soc. 102*, 554.
Szabo, A. G., Stepanik, T. M., Wayner, D. M., & Young, N. M. (1983) *Biophys. J. 41*, 233.
Tanaka, F., & Mataga, N. (1987) *Biophys. J. 51*, 487.
van Gunsteren, W. F., & Karplus, M. (1982) *Biochemistry 21*, 2259.
van Gunsteren, W. F., Swanminathan, S., Ichiye, T., & Karplus, M. (1982) *Biochemistry 21*, 5230.
Verlet, L. (1967) *Phys. Rev. 159*, 98.
Wahl, Ph. (1975) in *New Techniques in Biophysics and Cell Biology* (Smith, B., Ed.) Vol. 2, p 233, Wiley, New York.
William, R. J. P. (1979) *Biol. Rev. Cambridge Philos. Soc. 54*, 389.
Yamamoto, Y., & Tanaka, J. (1972) *Bull. Chem. Soc. Jpn. 45*, 1362.
Yu, H., Karplus, M., & Hendrickson, W. (1985) *Acta Crystallogr., Sect. B: Struct. Sci. B41*, 191.

Structural Organization of the Multienzyme Complex of Mammalian Aminoacyl-tRNA Synthetases†

Dianne E. Godar,‡ Douglas E. Godar,‡,§ Victor Garcia,‡ Alfredo Jacobo,‡ Ueli Aebi,‖ and David C. H. Yang*,‡
Department of Chemistry, Georgetown University, Washington, D.C. 20057, and Department of Anatomy and Cell Biology, Johns Hopkins University, Baltimore, Maryland 21205
Received December 8, 1987; Revised Manuscript Received February 29, 1988

ABSTRACT: The multienzyme complexes of mammalian aminoacyl-tRNA synthetases were purified from rat liver, rabbit liver, and rabbit reticulocytes according to the procedure slightly modified from Kellermann et al. [Kellermann, O., Brevet, A., Tonetti, H., & Waller, J.-P. (1979) *Eur. J. Biochem. 99*, 541–550]. Three forms of the synthetase complex with slightly different protein compositions were identified, suggesting a microheterogeneity of the synthetase complex. The hydrodynamic properties and the protein composition of the purified complexes were determined. The electron micrographs of the complex showed mostly amorphous particles and some hollow rings with an outer diameter of 164 Å and an inner diameter of 42 Å. The predicted hydrodynamic properties of several models of the complex were calculated. The properties of a ring model appear to best fit with those of the synthetase complex.

In mammalian cells, aminoacyl-tRNA synthetases including arginyl-, isoleucyl-, leucyl-, lysyl-, methionyl-, glutamyl-, glutaminyl-, and aspartyl-tRNA synthetases are physically associated as a high molecular weight multienzyme complex (Kellermann et al., 1979; Johnson & Yang, 1981; Sihag & Deutscher, 1984; Traugh & Pendergast, 1986). The synthetase complexes have been highly purified from several species, and the subunit molecular weights of the synthetases have been determined (Mirande et al., 1982a; Cirakoglu et al., 1985).

An increasing number of supramolecules have been found in mammalian cells, such as RNA polymerases (Sklar et al., 1975), ribonucleoprotein complexes [e.g., Walter and Blobel (1980) and Vincent et al. (1983)], and replicases (Noguchi et al., 1983). The association of mammalian aminoacyl-tRNA synthetases as a multienzyme complex has provided a model to explore the molecular evolution of the organization of such supramolecules. Recent demonstration of the direct involvement of tRNA in the ubiquitin- and ATP-dependent protein degradation pathway (Ferber & Ciechanover, 1987) underscores the importance of the elucidation of the metabolic compartmentalization of synthetases and tRNA in mammalian cells. A number of potential functions of the synthetase complex have been suggested (Deutscher, 1984). None has thus far been established.

The synthetase complexes are very labile and exhibit variations in size and activity [e.g., Dang and Yang (1979)]. The synthetases in the multienzyme complex appear to be associated loosely but specifically. As a consequence, it has been difficult to maintain the structure and the activities of the synthetase complex to establish its structural organization. The chromatograms and the sucrose gradient centrifugation profiles of the synthetase complex are usually broad and appear to represent collections of heterogeneous complexes [e.g., Dang and Yang (1979) and Kellermann et al. (1979)].

These observations have been attributed to endogenous proteolysis, partial dissociation of synthetases from the complex (Kellermann et al., 1979; Siddiqui & Yang, 1985), oxidation of sulfhydryl groups, or loss of non-protein components in the synthetase complex [e.g., Sihag and Deutscher (1983)] during its isolation (Dang & Dang, 1984). The instability of the synthetase activities further complicates the interpretation as to the enzyme composition of the synthetases in the complex.

† This work was supported by NIH Grant GM25848 (to D.C.H.Y.) and GM27765 (to U.A.). U.A. was also supported by a fellowship from the M. E. Müller Foundation of Switzerland.
‡ Georgetown University.
§ Deceased on June 12, 1987.
‖ Johns Hopkins University. Present address: M. E. Müller Institute for High Resolution Electron Microscopy at Biozentrum, University of Basel, CH-4056 Basel, Switzerland.

0006-2960/88/0427-6921$01.50/0